RELATING THE SPATIAL RESOLUTION AND SENSOR DEGRADATION OF DIWATA-2'S HIGH PRECISION TELESCOPE USING EDGE DETECTION

Fritz Rhaem M. Olivar[1*], Kristian R. Monay[1], Benjamin Jonah P. Magallon[1], Czar Jakiri S. Sarmiento[1]
[1]Training Center for Applied Geodesy and Photogrammetry, University of the Philippines Diliman
Diliman, Quezon City, Philippines
Email: fmolivar@stamina4space.upd.edu.ph

KEY WORDS: remote sensing, sensor degradation, edge detection, spatial resolution

ABSTRACT: Diwata-2 is a 56 kg microsatellite launched by the Philippines for earth observation last 2018. It is equipped with High Precision Telescope (HPT) which has four charge-coupled devices in the visible region (red, blue, and green), and in the near-infrared region. It also has a ground sampling distance of 4.7m at nadir. Due to its high spatial resolution, the HPT can be used for land cover change detection and disaster damage assessment. Having good image quality produced by the payload assures the usability of its product. However, the microsatellite has been in operation for almost three years and is constantly exposed to harsh space environments, which can result in sensor degradation. In order to maintain the image quality of the payload, it is necessary to observe the effects of degradation and apply proper adjustments and corrections. In this paper, occurrence of spatial degradation was investigated by using edge detection. This method was done by, first, clipping a part of an image with a distinguishable edge and homogenous sides. Examples of these are the roof of a building or road edges. Then, the mean pixel value of each row was computed from the clipped image and the pixel closest to the mean value per row was extracted. The edge was then delineated by connecting each extracted pixel location using linear regression. To compute the spatial resolution from the edge, pixel values perpendicular to it were extracted to produce an edge spread function. Then, the derivative of the edge spread function was computed to create a line spread function. To smoothen the curve, normalization and gaussian fitting was applied. The resulting function's full width at half max would indicate the image's spatial resolution. This represents the number of pixels the sensor needs to discern an object in an image. To further understand and differentiate the variations in spatial resolution, the pointing angle and the sun position relative to the satellite during image acquisitions were also considered.

1. INTRODUCTION

Diwata-2 was launched last October 29, 2018, as the second microsatellite of the Philippines following Diwata-1, having an altitude of 620 km with a sun-synchronous orbit. Diwata-2 has four payloads installed within its bus: the Middle Field Camera (MFC), a colored camera with a field of view of 189.3 by 141.9 km and a spatial resolution of 287.2m, the Enhanced Resolution Camera (ERC), a panchromatic camera with a field of view of 89.8 by 67.5 km and a spatial resolution of 54.6m; the Spaceborne Multispectral Imager (SMI) with Liquid Crystal Tunable Filter (LCTF), a camera with a spectral range of 440 nm to 1120 nm, a field of view of 83.7 by 62.7km and a spatial resolution of 126.9m; and the High Precision Telescope (HPT), an RGBNIR camera with a field of view of 3.1 by 2.3km and a spatial resolution of 4.7m. Currently, Diwata-2 has captured around 50,000 images which include images that covered 82.8% of the Philippines' land cover equivalent to 248,489.3 square kilometers, and also images of other places from different countries.

The microsatellite has been in operation for more than 3 years in low earth orbit just like its predecessor, Diwata-1. Being in low earth orbit, these microsatellites are exposed to stronger external disturbances some of these are from the sun, and the Earth's albedo and magnetic field (Magallon et al, 2018). These disturbances may not only cause its orbit degradation but also the degradation of its sensors that will lead to the degradation of its image quality. Lens point spreading, misfocus, motion, and atmospheric turbulence are the sources of image degradation and due to these factors, the images may experience blurring (Husein et al, 2019). The quality of images that are produced by the Diwata-2 sensors is vital for its operation as it is used mainly on earth observation and for disaster impact assessment. In order to monitor the image quality of the Diwata-2 images, image quality assessment through edge detection was applied to high-resolution images of the HPT payload.

Spatial resolution is the ability of a sensor to measure the smallest object, or the ground area captured for the instantaneous field of view (IFOV) of the sensor, or the linear dimension on the ground represented by each pixel (Liang et al., 2020). The spatial resolution of a satellite image depends primarily on the distance between the target and the sensor, and its IFOV, which determines the visibility of the sensor in the earth's surface at a given altitude at a particular time (Gopi et al., 2007). Lower value of a spatial resolution means that it has less blurring and more details in the image are seen compared to higher values of spatial resolution. Spatial resolution degradation means

that the spatial resolution of the images produced by a sensor has increased in value, e.g. from 0.25m to 5m. (Hubert et al.,2012).

The image quality assessment of high-resolution images is commonly done through the extraction of the Modulation Transfer Function (MTF) of images (Zhaocong et al, 2018). MTF is produced by applying Fourier transformation in the Linear Spread Function (LSF), which is obtained by deriving the Edge Spread Function (ESF) (Zwanenberg et al, 2019). Studies using edge detection are commonly found due to its fast and efficient processing of the MTF (Estribeau et al, 2004). For this study, we used the approach of Crespi et al., (Crespi et al, 2009) which uses an edge detection method to estimate the spatial resolution of an image by extracting the Full-Width at Half Max (FWHM) from the LSF.

The team monitored the change in the value of the FWHM from the first quarter of 2019 to the present. For the purposes of the study, the solar elevation angle is defined as the angle of the sun from the horizon for a specific area and the solar azimuth angle is referred to from the North. Likewise, the satellite view altitude is defined as the angle from the satellite's horizon to the point of interest, and the satellite view azimuth is referred to from the satellite's velocity vector. Sun range is the distance between the target and the sun, satellite range is the distance between the target and the satellite, and the ground distance is the distance between the satellite's nadir and the target. The relationship of the FWHM towards the sun angle, viewing angle, satellite range, sun range, and ground distance of the satellite and the target during the image acquisition is also observed in this study. The sun angle, viewing angle, sun range, satellite range, and ground distance at the time of the image capture were extracted from Skyfield Python Library using propagation. This study is conducted on HPT images of the Diwata-2 satellite to assess the health of this payload and to address the need for its calibration.

2. METHODOLOGY

This assessment is mainly based on the ability of the payload to distinguish an edge in an image. The first step in the process is to clip a straight edge from the image, this edge must be visually discernible, common examples of these are the edge of a building or the side of the roads. Edge detection is then applied to the clipped image, this is done by finding the pixel within the row of the image which is closest to the mean value of the pixel values in the same row. After determining the edge pixel per row, linear regression is applied to delineate the edge in the clipped image. The edge profiles of these edge points were extracted by obtaining 5 pixels from each side of the edge by creating lines from the edge points perpendicular to the linearly regressed edge line. Cubic spline interpolation was applied to the points before extracting the edge profiles. The ESF is derived from the mean value of the edge spread profile. The LSF is then obtained from the derived ESF. Our team used gaussian fitting to smoothen the function to determine the FWHM value. This value signifies the number of pixels that are needed for that image to discern an edge. The lower the value of the FWHM, the better the resolution of the image. The flow chart of the edge detection process can be seen on Figure 1. The sun angle, viewing angle, satellite range, sun range, and ground distance were then extracted through orbit propagation using Skyfield Python Library.

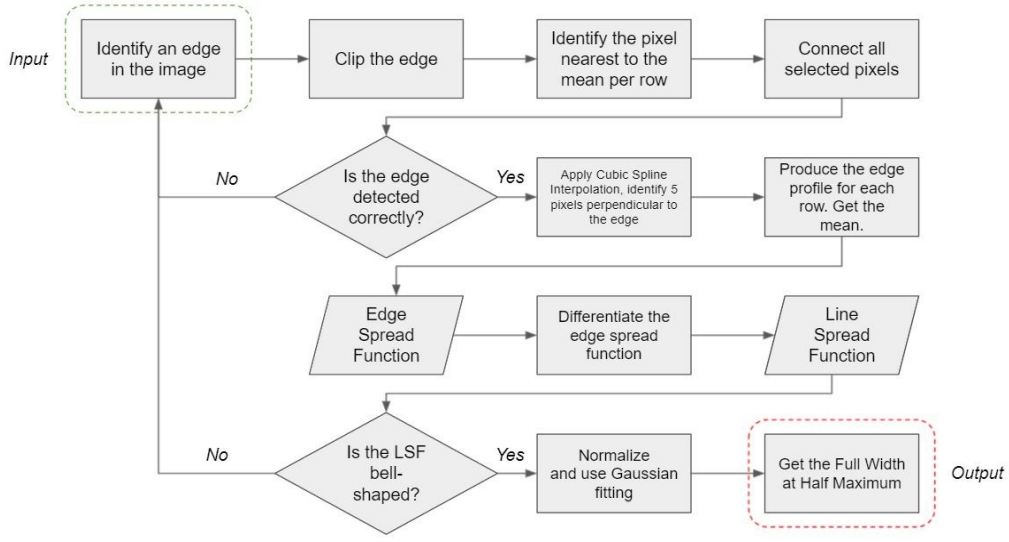

Figure 1. Flow Chart of the Edge Detection Method

2.1 Edge selection and clipping

The blurring assessment process begins by selecting a straight edge in the image, see Figure 2. The edge must be vertical, it may be a roof of a structure or an edge of a road or a crop field if it remains to be homogenous on both sides of the edge. The edge must be close to the image center as much as possible. The clipping process is done through Quantum Geographic Information System (QGIS) by using its clipping tool.

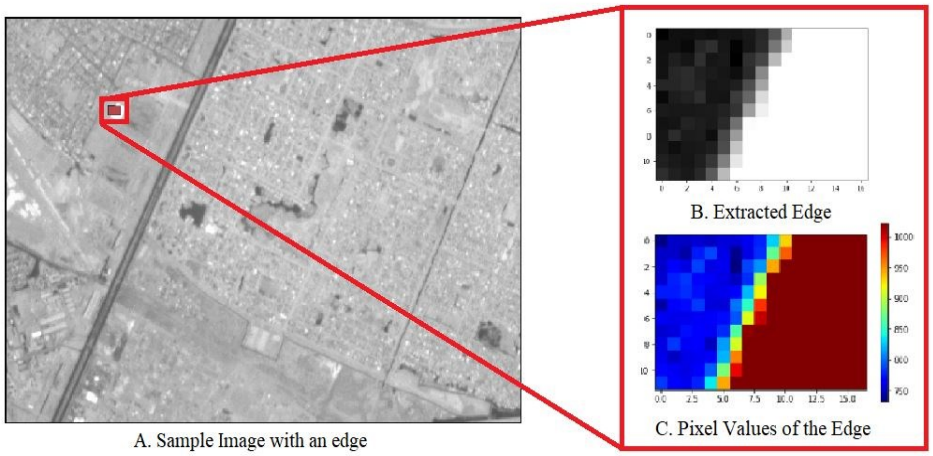

Figure 2. Sample edge selection

2.2 Spatial Resolution Extraction through Edge Detection Algorithm

2.2.1 Edge detection

From this point on, Python programming language is used to conduct the steps in the edge detection process. The next step for the assessment is edge detection. This is done by determining the pixel which is closest to the mean of the pixel values for every row, see Figure 3. The identified position of the edge per row is then linearly regressed to delineate the edge in the clipped image, see Figure 4. If the edge detected from the algorithm is not collinear, see Figure 5, we will have to select another edge until it becomes collinear. If the edge points are not collinear, the regressed edge will appear skewed thus it will not correctly represent the edge in the region of interest.

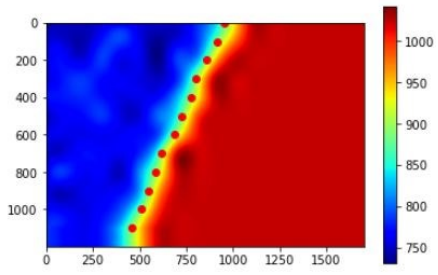

Figure 3. Edge point determination per row

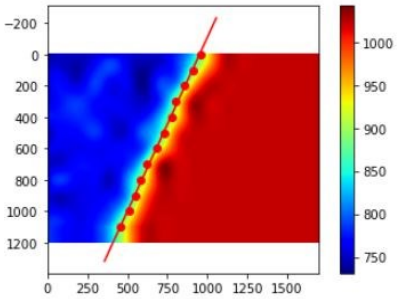

Figure 4. Edge delineation

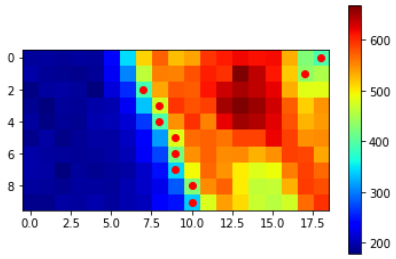

Figure 5. Non-collinear edge points

2.2.2 Cubic Spline Interpolation and Edge Spread Profile Extraction

Cubic spline interpolation was applied to the sampled pixels before extracting the edge profiles, see figure 6. We used scipy.interpolate python library for the interpolation (Virtanen et al., 2020). After obtaining the edge location in the clipped image, a total of 11 sample pixels are selected from the perpendicular lines created from the edge points per row. These 11 points are from 5 sample pixels from each of the homogenous sides and the edge point itself, see Figure 6.

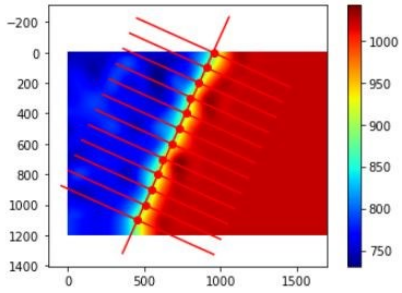

Figure 6. Sample pixel value extraction

2.2.4 Edge Spread Function

Edge profiles of the sampled pixels from the perpendicular lines are extracted and graphed by their pixel value,see Figure 7. The Edge Spread Function is then derived from the mean of the 11 corresponding pixels, as shown by the blue line below.

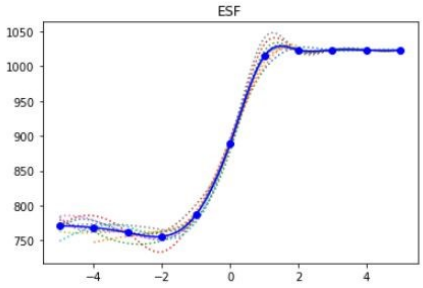

Figure 7. Edge Spread Function

2.2.5 Linear Spread Function

The Linear Spread Function, see Figure 8, is derived by differentiating the Edge Spread Function. This function will be used to determine the Full width at Half Max which signifies the number of pixels that are needed to discern an edge. If the LSF does not follow a normal distribution nor if it's not bell-shaped, see Figure 9, we will have to select another edge as this will give an erroneous value for its FWHM.

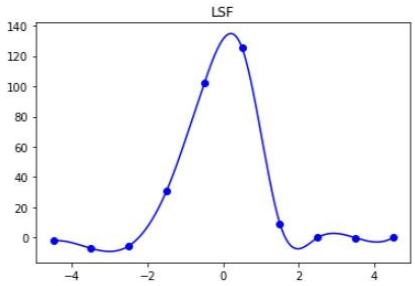

Figure 8. Linear Spread Function

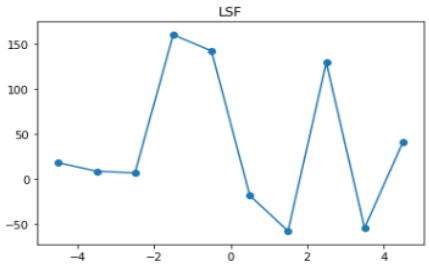

Figure 9. Erroneous Linear Spread Function

2.2.6 Normalization

Normalization is done to determine the half value of the LSF since the value of the function is still in terms of the difference in the pixel values of the edge profile, see Figure 10. This process is done to make the computation for the FWHM easier.

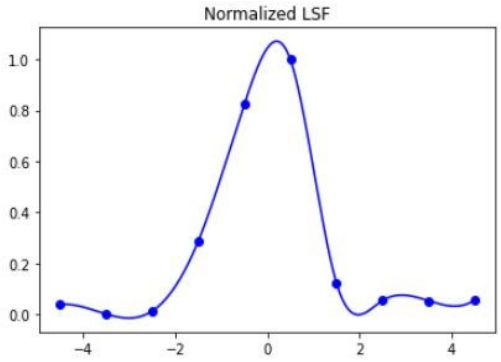

Figure 10. Normalization of the Linear Spread Function

2.2.7 Gaussian Fitting

It is recommended to perform a Fermi Logistic Function to remove the noises in the ESF to obtain a smooth and fitted LSF (Li et al., 2009). Due to having inconsistent effects in our data by applying Fermi Logistic Function to our ESF, our team applied Gaussian fitting, see Figure 11, to the normalized curve in order to smoothen the curve of the LSF instead. By doing this, the approximation of the value of the full width at half max is not overfitted and is close to the actual value based on the linear spread function.

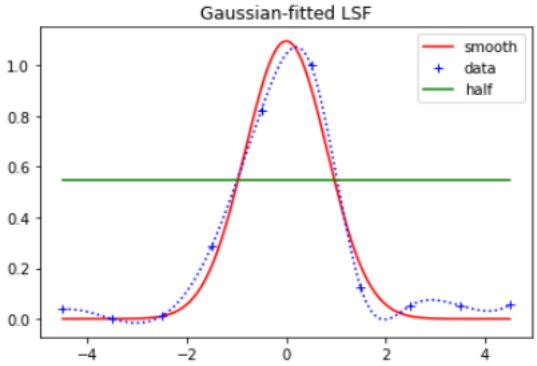

Figure 11. Gaussian Fitted and Normalized LSF

2.2.8 Full Width at Half Max

Lastly, the value of full width at half max is computed by obtaining the value of the space between the half max (0.5 value) of the function. This value corresponds to the number of pixels needed to define the edge in that image, thus representing the spatial resolution of the image.

2.3 Extraction of the Viewing Angle, Sun Angle, Satellite Range, Sun Range, and Ground Distance

The team created a script using Skyfield's Python Library (Rhodes, 2020) to propagate the orbit of Diwata-2 at the time of the image capture to extract and compute the viewing angle, sun angle, satellite range, sun range, and ground distance. We used Local Vertical Local Horizontal as the reference frame in this script. We then used the computed values to see if there is a correlation between them and the FWHM value.

3. RESULTS

The team obtained a total of 61 edges, all of them are man-made natural edges (buildings, croplands, etc.), from the start of its operation to the 2nd quarter of 2021. This low number of edges is due to the fact that not every image capture mission of the Diwata-2 has a straight edge that can be used in this study. From the 61 values of FWHM, which is considered as the spatial resolution of the images, the mean of the values is 2.3676m with a standard deviation of 0.4311. This means that an image has an average of 2-3 pixels to manifest an edge. The spatial resolution values were grouped into 5 groups depending on the ground distance; 0-25km, 25-50km, 50-75km, 75-100km, and the ranges greater than 100km; 21 edges had 0-25km ground distance, 17 edges had 25-50km ground distance, 13 edges had 50-75km ground distance, 4 edges had 75-100 ground distance, and 6 edges had greater than 100km ground distance. These values are then correlated in line graphs and scatter plots with the mission's date, local time, sun altitude angle, sun azimuth angle, view altitude angle, and the view azimuth angle to see if there is a trend between these values and the spatial resolution.

Figure 12, as shown below, represents the line graph of the spatial resolution versus the date of the missions. There is no significant increase in FWHM values throughout the life of Diwata-2. The spatial resolution of the images from the missions of Diwata-2 remains within 2-3m from 2018 up to the present. It can also be seen that there is more data found in 2021 because the missions are much more frequent in this year compared to the previous years.

Figure 13, as shown below, represents the line graph of the spatial resolution versus the local time. All the missions were captured between 1:00 PM to 3:00 PM in local time of the target place of the satellite. There is no apparent trend in this graph.

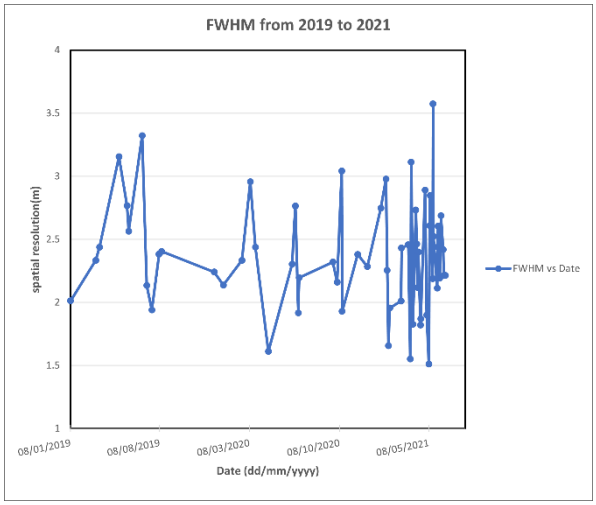

Figure 12. Spatial resolution vs Date of the missions

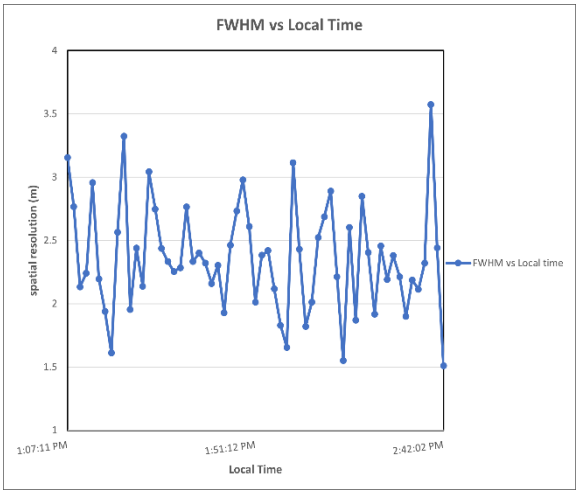

Figure 13. Spatial resolution vs Local Time

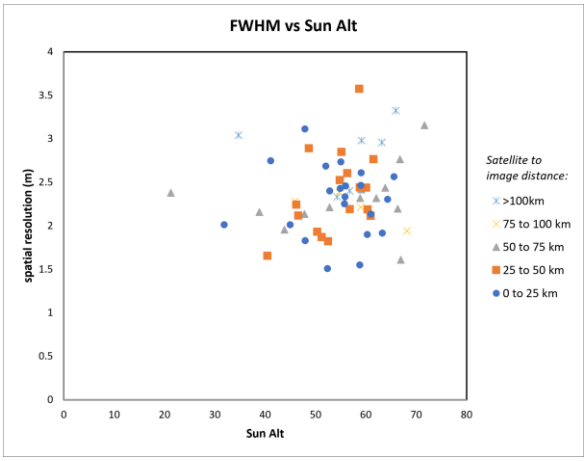

Figure 14. Spatial resolution vs Sun Alt Angle

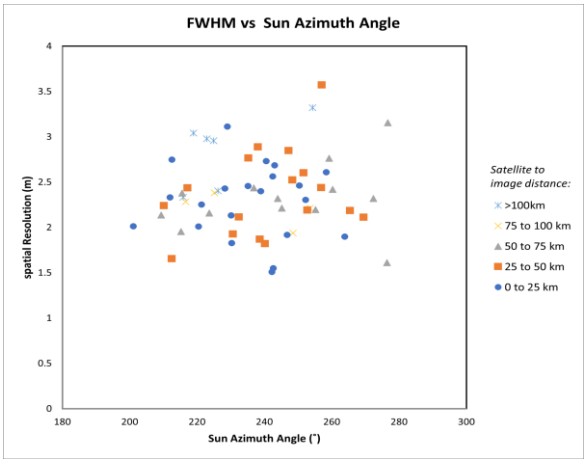

Figure 15. Spatial Resolution vs Sun Az Angle

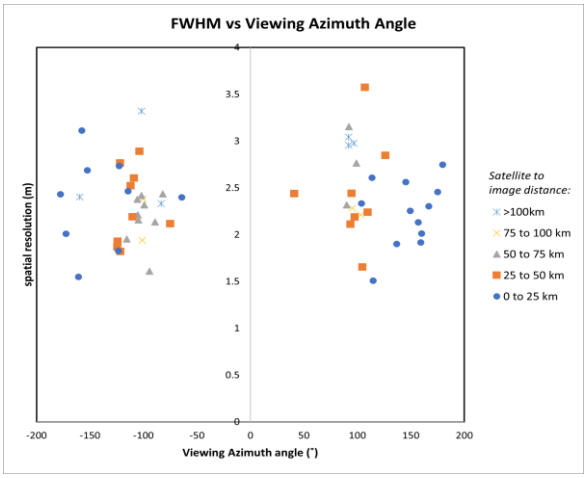

Figure 16. Spatial Resolution vs View Az Angle

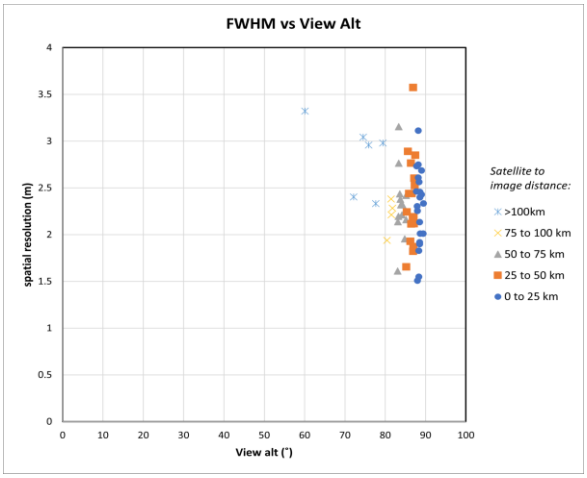

Figure 17. Spatial Resolution vs View Alt Angle

Figure 14 represents the scatter plot of the spatial resolution versus the Sun Altitude Angle. Majority of the data are between 40-70 degrees this is because most of the missions are taken from 1:00PM to 3:00PM in local time of the target location. There is no apparent trend on this graph too.

Figure 15 represents the scatter plot of the spatial resolution versus the Sun Azimuth Angle. It can also be seen that there is no apparent trend in the data in this as well.

Figure 16 represents the scatter plot of the spatial resolution versus the View Azimuth Angle. In this graph, the data is spread on the negative and positive sides of the graph with no apparent trend as well.

Figure 17 represents the scatter plot of the spatial resolution versus the View Altitude Angle. It can be seen in this graph that most of the data are found between 80-90 view alt angles, this signifies that most of the missions of Diwata-2 that have captured an edge are nadir or off-nadir. It is also apparent that there is no trend within the data.

Based on the line graphs and scatter plots above, there is no definite correlation between the spatial resolution of the images to the values it was compared to. To confirm this, we extracted the correlation coefficients between the date the image was taken, the view altitude angle, the view azimuth angle, the sun altitude angle, and the sun azimuth angle versus the spatial resolution while also considering the grouping of the ground distance between the satellite and the target, as shown in the table below.

Table 1. Correlation Coefficients

Ground Distance	Correlation Coefficients vs FWHM				
	Date	View Alt	View Az	Sun Alt	Sun Az
0-25km	0.0483	-0.0725	-0.1257	-0.0440	-0.0666
25-50km	0.2216	0.2168	0.1732	0.4455	0.3050
50-75km	-0.2585	-0.1204	0.5581	0.2679	0.2728
75-100km	0.4915	0.8867	0.2644	-0.8019	-0.6503
>100 km	0.1134	-0.4939	0.4651	0.1065	0.6215
All the data	-0.0309	-0.3330	0.0864	0.1395	0.0906

The range of the value of a correlation coefficient is from -1 to 1, where being close to -1 indicates that it has a negative correlation, being close to 1 indicates that it has a positive correlation and being close to 0 indicates that it has little to no correlation. Having a positive correlation means that if a value is increasing the other value is increasing as well while having a negative correlation means that if a value is increasing the other value is decreasing. For the data having a ground distance of 0-25km with 21 data points, the values in the correlation coefficient table indicate that all the values have no correlation because their values are close to 0. For the data having a ground distance of 25-50 km with 17 data points, the correlation between the sun altitude angle indicates a weak positive correlation, while the other correlated values indicate no correlation. For the data having a ground distance of 50-75 km with 13 data points, the correlation between the view azimuth angle indicates a weak positive correlation, while the other correlated values indicate no correlation. For the data having a ground distance of 75-100km with 4 data points, the correlation between the date of the mission indicates a weak positive correlation, between the view altitude angle indicates a positive correlation, between the sun azimuth angle indicates a negative correlation, between the sun azimuth angle indicates a weak negative correlation, while the correlation between the view azimuth angle established no correlation. For the data having a ground distance of more than 100km with 6 data points, the correlation between the view altitude angle indicates a weak negative correlation, between the view azimuth angle indicates a weak positive correlation, between the sun azimuth angle indicates a positive correlation, while the remaining correlated values indicate no correlation. Lastly, when considering the correlation of all the data, none of them exhibits a correlation with one another. The inconsistencies of these correlations might be due to the different sample size of each category; the group of 75-100km, and greater than 100km, having sample sizes of 4 and 6 respectively, had produced correlations while the other groups produced little to none. Based on the graphs and tables above, there is no established correlation between the variables observed and the spatial resolution of the images.

4. CONCLUSION

One of the main reasons for the inconsistency in the data could be from the edges that were extracted from the images were all from natural edges (buildings, roads, croplands, etc.). According to Crespi et al., (Crespi et al., 2009), natural edges might have more noise than actual targets that are appropriate for calibration. While there was no established correlation between the variables observed, the spatial resolution values did not indicate a significant increase which means that for now the effects of sensor degradation is minimal. For further studies, it is recommended that there must be a specific mission that targets proper calibration sites; an alternative for this would be to recapture places with extracted FWHM to see if there is a significant change in the FWHM value. Moreover, it is also recommended to explore the extraction of the MTF to further advance the assessment of the images from the Diwata-2 sensors.

5. REFERENCES

Crespi, M., De Vendictis, L., 2009. A Procedure for High-resolution Satellite Imagery Quality Assessment. Sensors, Basel, Switzerland, 9(5), pp. 3289-3313. doi.org/10.3390/s90503289.

Estribeau, M., Magnan, P., 2004. Fast MTF measurement of CMOS imagers at the chip level using ISO 12233 slanted edge-methodology. Proceedings of SPIE - The International Society for Optical Engineering. doi: 10.1117/12.565503

Hussein, M. S., Hanafy, M. E., Mahmoud, T. A., 2019. Characterization of the sources of degradation in remote sensing satellite images. International Conference on Innovative Trends in Computer Engineering (ITCE), 2019, pp. 29-34, doi: 10.1109/ITCE.2019.8646604.

Gopi, S., Sathikumar, R., Madhu, N., 2007. Advanced Surveying Total Station, GIS, and Remote Sensing. Delhi, India, pp. 317-318.

Hubert, S., Schwarzer, S., Jaquet, J-M, 2012. Spatial Degradation of Classified Satellite Images. The Open Remote Sensing Journal, 2012, 5, pp.64-72, doi: 10.2174/1875413901205010064.

Li, T., Feng, H., Xu, Z., Li, X., Cen, Z., Li, Q., (2009). Comparison of different analytical edge spread function models for MTF calculation using curve-fitting. Proceedings of SPIE - The International Society for Optical Engineering, vol. 7498. doi:10.1117/12.832793

Liang, S., Wang, J., 2020. Advanced Remote Sensing (Second Edition), Chapter 1 - A systematic view of remote sensing, pp. 1-57. doi.org/10.1016/B978-0-12-815826-5.00001-5. from https://www.sciencedirect.com/science/article/pii/B9780128158265000015.

Magallon, B. J. P., Labrador, J. L. D., Gonzalez, A. N., Felicio, F. M. B., Tupas, M. E. A, 2018. Diwata-1 Target Pointing Error Assessment using orbit and space environment prediction model. IEEE International Conference on Aerospace Electronics and Remote Sensing Technology (ICARES), 2018, pp. 1-7, doi: 10.1109/ICARES.2018.8547062.

Rhodes, Brandon. Skyfield Python Library, last visited August 2021, from http://rhodesmill.org/skyfield/. 2019ascl.soft07024R

Virtanen, P. Gommers, R., Oliphant, T. E., Haberland, M., Reddy, T., Cournapeau, D., Burovski, E., Peterson, P., Weckesser, W., Bright, J., van der Walt, S. J., Brett, M., Wilson, J., Millman, K. J., Mayorov, N., Nelson, A. R. J., Jones, E., Kern, R., Larson., E., Carey, C. J., Polat., I., Feng, Y., Moore, E. W., VanderPlas, J., Laxalde, D., Perktold, J., Cimrman, R., Henriksen, I., Quintero, E. A., Harris, C. R., Archibald, A. M., Riberio, A. H., Pedregosa, F., van Mulbregt, P., and Scipy 1.0 Contributors, 2020. Scipy 1.0: Fundamental Algorithms for Scientific Computing in Python. Nature Methods, vol. 17, pp. 261-272. doi: 10.1038/s41592-019-0686-2. from https://docs.scipy.org/doc/scipy/reference/generated/scipy.interpolate.CubicSpline.html.

Zhaocong, W., Zhipeng, L., Yi, Z., Feifei, G., Lin, H. 2018. Image Quality Assessment of High-resolution Satellite Images With MTF-based Fuzzy Comprehensive Evaluation Method. ISPRS-International Archives of the Photogrammetry, Remote Sensing and Spatial Information Sciences. XLII-3. Pp. 1907-1914. Doi: 10.5194/isprs-archives-XLII-3-1907-2018.

Zwanenberg, O. van., Triantaphillidou, S., Jenkin, R., Psarrou, A, 2019. Edge Detection Techniques for Quantifying Spatial Imaging System Performance and Image Quality. IEEE/CVF Conference on Computer Vision and Pattern Recognition Workshops (CVPRW), 2019, pp. 1871-1879, doi: 10.1109/CVPRW.2019.00238.